

Modeling Modern Methane Emissions from Natural Wetlands

1. Model Description

Bernadette P. Walter¹, Martin Heimann², and Elaine Matthews¹

¹Columbia University/NASA Goddard Institute for Space Studies, New York

²Max-Planck-Institut für Biogeochemie, Jena, Germany

Abstract. Methane is an important greenhouse gas which contributes about 22% to the present greenhouse effect. Natural wetlands currently constitute the biggest methane source and were the major one in pre-industrial times. Wetland emissions depend highly on the climate, i.e., on soil temperature and water table. In order to investigate the response of methane emissions from natural wetlands to climate variations, a process-based model that derives methane emissions from natural wetlands as a function of soil temperature, water table, and Net Primary Productivity is used. For its application on the global scale, global data sets for all model parameters are generated. In addition, a simple hydrologic model is developed in order to simulate the position of the water table in wetlands. The hydrologic model is tested against data from different wetland sites, and the sensitivity of the hydrologic model to changes in precipitation is examined. The global methane-hydrology model constitutes a tool to study temporal and spatial variations in methane emissions from natural wetlands.

1. Introduction

Methane is one of the important greenhouse gases and plays an important role in atmospheric chemistry. Its contribution to the current greenhouse effect is about 22% [Lelieveld *et al.*, 1998]. Ice core records show that the atmospheric methane concentration has varied between 350 ppbv and 700 ppbv during the last 220,000 years until the beginning of industrialization [Jouzel *et al.*, 1993]. Changes in methane concentrations parallel changes in the atmospheric temperature which are inferred from variations in the $\delta^{18}\text{O}$ value. Evidence has been found that at the end of the Younger Dryas methane increases in Greenland lag the drastic temperature increase by up to a few decades [Severinghaus *et al.*, 1998; Severinghaus and Brook, 1999] suggesting a response of wetland emissions to a climatic change. These climate-induced changes in wetland emissions comprise changes in wetland area and distribution, and changes in methane fluxes, as wetlands are a highly climate-sensitive methane source. Since the beginning of the industrialization the atmospheric methane concentration has increased by

a factor of 2.5 and is now 1750 ppbv. In the last 2 decades atmospheric methane concentrations have continued to increase and superimposed on this trend is considerable interannual variation [Dlugokencky *et al.*, 1998]. The dramatic increase in the last 200 years has mainly been caused by human activities, though wetlands are believed to contribute considerably to interannual variations and particular anomalies (Hogan and Harris [1994], section 3.3.1 and 3.5 of Walter *et al.* [this issue]).

In this article a global process-based, climate-sensitive model to study climate-induced variations in methane emissions from natural wetlands is presented. The model is based on a 1-dimensional model that has been tested thoroughly against high-frequency time series of observations from 6 different wetlands [Walter *et al.*, 1996; Walter and Heimann, 2000]. The only other global process-based model in the literature was developed by Cao *et al.* [1996]. It calculates present-day global methane emissions from wetlands based on the amount of decomposed organic carbon, water table and temperature. However, their model has never been tested against time series of methane emission data and not been applied to temporal variations. In section 2 the methane model and its application on the global scale are described. Section 3 covers global data sets used. The global wetland distribution is prescribed from the data set of Matthews and Fung [1987]. Global data sets of all model parameters, which are soil depth, rooting depth, relative pore space, and efficiency of plant-mediated transport, are developed from existing global data sets of vegetation [Wilson and Henderson-Sellers, 1985] and soil characteristics [Dunne and Wilmott, 1996]. In section 4 the hydrologic model to derive the variation of the water table in wetlands is presented. This includes a model description, tests against observational data, sensitivity test and global model results of the hydrologic model.

2. The Methane Model

For global model runs the 1-dimensional methane model of Walter and Heimann [2000] is applied to the global wetland distribution of Matthews and Fung [1987]. Figure 1 shows a schematic of the methane model. The model forcing consists of daily water table, soil temperature and Net Primary Productivity (NPP). The processes of methane production in the anoxic soil, methane oxidation in the oxic soil, and transport of methane by diffusion, ebullition and through plants are modeled explicitly in a soil column. The model calculates methane concentration profiles in the soil and methane emissions to the atmosphere on a daily basis [Walter and Heimann, 2000]. Methane production occurs in the anoxic soil between soil depth and water table; production rates depend on substrate availability and soil temperature. Methane oxidation takes place in the oxic soil between water table and soil surface; oxidation

rates are controlled by methane concentrations in the soil (using the Michaelis-Menten equation) and soil temperature. Diffusion occurs through the water- or air-filled soil pores and depends on the vertical methane concentration gradient (using Fick's first law) and the relative pore space. Ebullition only takes place in the water-saturated soil where bubbles are formed and rise to the water table. Plant-mediated transport, which is the transport of methane through the stems of plants, occurs from all soil layers above the rooting depth. It is influenced by the type of vegetation present, which is characterized by the parameter T_{veg} describing the efficiency of plant-mediated transport at a grid cell. Plant-mediated transport varies also as a function of the growing state of plants, which is modeled as a function of soil temperature.

The methane production rate, R_{prod} , is influenced by soil temperature and NPP, which is taken as a measure of availability of organic carbon for methane production. R_{prod} is parameterized in the following way:

$$R_{prod} = R_0 \cdot f(NPP) \cdot f(T_{soil}(t) - T_{mean}) \quad (1)$$

$f(NPP)$ is a function describing the seasonal availability of organic carbon for methane production as well as its distribution with depth. The variation of $f(NPP)$ with time is a function of the relative changes in NPP with time; the vertical distribution of $f(NPP)$ depends on the rooting depth and is constant with time. $f(T_{soil}(t) - T_{mean})$ describes the time evolution of the soil temperature using a Q_{10} dependency ($Q_{10}=6$), whereas $T_{soil}(t)$ is the soil temperature at time t and T_{mean} is the annual mean soil temperature. R_{prod} is zero at sub-zero temperatures.

The parameter R_0 is a measure of the amount and quality of substrate for methanogenesis. As the processes determining R_0 are not modeled explicitly R_0 was adjusted to each of the 6 data sets used to test the model. For the global application of the model the value of R_0 for each grid cell, $R_0(x,y)$, is determined using simple multiple linear regression based on the following assumptions. The availability of substrate for methane production is assumed to depend on (1) the amount of easily decomposable soil organic matter and (2) the annual mean temperature. (1) The amount of easily decomposable organic matter (from litter production, dead fine roots and root exudates) is assumed to be connected with NPP. Hence, the total annual NPP at a grid cell, $NPP_{tot}(x,y)$, is used as a measure of substrate availability. $NPP_{tot}(x,y)$ is taken from the global terrestrial carbon cycle model Biosphere-Energy Transfer and Hydrology (BETHY) [Knorr, 199.] which calculates NPP for a suite of vegetation types derived from the vegetation

map of *Wilson and Henderson-Sellers* [1985]; wetlands are one of the types and are distinguished by an absence of water stress. However, a large fraction of locations identified as wetlands by *Matthews and Fung* [1987] are not primarily wetlands in the vegetation map of *Wilson and Henderson-Sellers* [1985]; wetlands in the vegetation map of *Wilson and Henderson-Sellers* [1985] usually coincide with high fractional inundation in the data set of *Matthews and Fung* [1987] though. Hence, in most cases the NPP values from the BETHY model are for non-wetland ecosystems which constitutes an inconsistency; however, errors are only expected in regions with substantial water stress. (2) The annual mean temperature of the upper 20 cm of soil, $T_{\text{mean}}(x,y)$, is taken as a measure of the soil decomposition rate and hence the production rate of substrate for methanogenesis. Using the R_0 values in combination with the respective NPP_{tot} and T_{mean} values from the 6 test sites of the methane model $R_0(x,y)$ is determined. A simple multiple linear regression yields:

$$R_0(x,y) = 0.45 - 0.1 \cdot \frac{T_{\text{mean}}(x,y)}{[^\circ\text{C}]} - 0.001 \cdot \frac{\text{NPP}_{\text{tot}}(x,y)}{[\text{gC} \cdot \text{m}^{-2} \cdot \text{yr}^{-1}]}, \quad (2)$$

which shows that $R_0(x,y)$ is mainly dependent upon $T_{\text{mean}}(x,y)$. Calculating $R_0(x,y)$ this way considers only substrate quantity. However, substrate quality and the chemical conditions in soil, such as redox potential, pH and the presence of competing electron acceptors also affect methane production rates, and thus R_0 . A process-based model to predict R_0 from the above mentioned parameters would hence be useful. However, no such model is yet available, partly due to limited knowledge about the quantitative relationships between these parameters and R_0 , and because sufficient data on the global distribution of factors affecting R_0 are lacking. However, as more data become available, a model like that proposed by *Valentine et al.* [1994] and *Holland* [unpublished] could be used to predict R_0 globally.

Figure 2 summarizes model components, forcing data and global data sets used for the global model run; the spatial resolution is 1° by 1° . As mentioned above the global wetland distribution is taken from the data set of *Matthews and Fung* [1987]. Global data sets of plant-mediated transport, T_{veg} , rooting depth, n_{root} , soil depth, n_{soil} , and relative pore space, f_{coarse} , are derived from existing data sets as described in section 3. A simple hydrologic model is developed to simulate the water table in wetlands which will be described in section 4. The model forcing consists of soil temperature at several soil depths and NPP (for the methane model), and surface net solar radiation, 2m (air-)temperature, and precipitation (for the hydrologic model).

3. Global Data Sets

3. 1. Global Wetland Distribution

The global distribution of natural wetlands is taken from the data set of *Matthews and Fung* [1987] that gives the percentage of wetlands within each 1° by 1° grid cell. Figure 3 shows global wetland areas derived from that data set. However, the data set does not account for seasonal or even interannual variations of wetland areas and the wetland area given is considered to be the maximum area. The hydrologic model (section 4) simulates the seasonality of the water table at wetland sites and hereby introduces some seasonality. For example, in tropical wetlands soils dry for a certain period of time, i.e., in the model there is no wetland during the dry season (Figure 7, Panama). However, expansion and contraction of wetland areas are not accounted for.

3. 2. Global Vegetation Distribution

The global 1° by 1° land cover data set by *Wilson and Henderson-Sellers* [1985] is used to derive all vegetation-dependent parameters. These parameters are the quality of plant-mediated transport, T_{veg} , the rooting depth, n_{root} , and the soil depth, n_{soil} (Figure 2). *Wilson and Henderson-Sellers* define 53 land cover types and to each of them relative fractions of 24 possible vegetation types (in the following referred to as WH-vegetation types) are assigned. That means a grid cell can be covered by different fractions of different WH-vegetation types. Combining the 24 WH-vegetation types, as shown in Appendix A, reduces the number of vegetation types to the following 8: tree, shrub, short grass, long grass, tundra, swamp, bare soil and other. The vegetation type other comprises non-natural “vegetation” types such as urban or arable lands. Essentially, the distinction between different types of trees and shrubs is ignored because it is not important for determining the parameters T_{veg} , n_{root} , and n_{soil} .

3. 3. Plant-mediated Transport, T_{veg}

The knowledge about the efficiency of plant-mediated transport by different vegetation types is sparse. Some plants are known to be good transporters of gas. Examples include rice plants [*Schütz et al.*, 1989], *Eriophorum angustifolium* [*Schimel*, [1995]; Peter Frenzel, personal communication, 1994) or *Scheuchzeria palustris* [*Shannon et al.*, 1996]. While a few plants have been examined for their gas-conducting properties, little is known about the gas-conducting properties of most wetland plants. Therefore, several assumptions have been made in this study (P. Frenzel, personal communication, 1998). It is assumed that plants found growing in wetlands tend to have gas-conducting systems to supply O_2 to their roots, which are often in saturated soil. The vegetation types grasses, tundra and swamp are considered to have a high potential for plant-mediated transport. Trees, however, do not seem to be good

conductors, with the exception of mangroves [Ramachandran and Ramachandran, 1998]. Shrubs are assumed not being capable of transporting gas through their wood stems. Based on information on vegetation and plant-mediated transport available for the test sites of the methane model [Walter and Heimann, 2000] the unitless parameter T_{veg} , characterizing the efficiency of plant-mediated transport, was defined to range between 0 and 15. T_{veg} of 0 means no plant-mediated transport, 1 poor and 15 very good plant-mediated transport, respectively. T_{veg} values that were assigned to each vegetation type are summarized in Table 1. The global distribution of $T_{veg}(x,y)$ is obtained by weighting the T_{veg} values of each vegetation type, $T_{veg,i}$, with the relative coverage of each vegetation type $p_i(x,y)$ in a grid cell:

$$T_{veg}(x, y) = \frac{\sum_{i=1}^7 p_i(x, y) \cdot T_{veg, i}}{\sum_{i=1}^7 p_i(x, y)} . \quad (3)$$

Only vegetation types 1-7 are considered for natural wetlands since vegetation type 0 does not occur over the distribution of *Matthews and Fung's* wetlands. Figure 4a shows the global distribution of the parameter T_{veg} in wetlands.

3. 4. Rooting Depth, $nroot$

The rooting depth, $nroot$, is derived from the vertical distribution of the root biomass for different vegetation types given by *Jackson et al.* [1996]. They used an asymptotic, nonlinear equation to describe the cumulative root fraction $Y(z)$ at depth z . This equation, taken from a model of vertical root distribution [Gale and Grigal, 1987] is used here:

$$Y(z) = 1 - \beta^z , \quad (4)$$

where β is an extinction coefficient. β values for vegetation types, taken from *Jackson et al.* [1996], were derived from soil studies and biome analyses. The vegetation types used in *Jackson et al.* [1996] are assigned to vegetation types 1-6 used in this article (Table 2). The rooting depths of the vegetation types 0, other, and 7, bare soil, are set to 0 cm. From the five β values for forest biomes in *Jackson et al.* [1996] five rooting depths are calculated and averaged to obtain the rooting depth of vegetation type 1, tree. For vegetation type 6 (swamp) the β value for temperate grassland is used because most areas denoted as swamps by *Wilson and Henderson-Sellers* [1985] are located in higher latitudes. The rooting depth $nroot_i$ in cm

for each vegetation type i is derived by cutting off the cumulative root distribution $Y_i(z)$ in each vegetation type at 90%. Thus, $nroot_i$ is obtained by:

$$nroot_i = \frac{\ln(1 - Y_i(z))}{\ln \beta} \quad Y_i(z) = 0.9 . \quad (5)$$

Table 1 lists the resulting rooting depths. They are comparable to rooting depth observations at the test sites of the methane model [Walter and Heimann, 2000]. The rooting depth $nroot_i$ of each vegetation type i is weighted by the relative coverage of each vegetation type $p_i(x,y)$ in a grid cell and by $T_{veg,i}$ because the rooting depth is mainly relevant for plant-mediated transport. Hence, the rooting depth $nroot(x,y)$ of a grid cell is calculated from:

$$nroot(x, y) = \frac{\sum_{i=1}^6 p_i(x, y) \cdot T_{veg, i} \cdot nroot_i}{\sum_{i=1}^6 p_i(x, y) \cdot T_{veg, i}} . \quad (6)$$

Figure 4b shows the global distribution of rooting depths of wetlands obtained by this method.

3. 5. Soil Depth, $nsoil$

The soil depth, $nsoil$, is the lower boundary of the active layer of the methane model, which is that part of soil where methane production occurs. In the methane model, it is assumed that methane is mainly produced from fresh organic material, incorporated in the soil as litter, root exudates, and dead fine roots. Therefore, the depth of the active layer, $nsoil$, is linked with the vertical root distribution. Hence, $nsoil$ is also calculated from the cumulative root fraction $Y(z)$. To obtain $nsoil$, $Y(z)$ is truncated at 99%, because the active layer depth is deeper than the rooting depth due to downward transport of organic matter. The soil depth of vegetation types 0 and 7 is set to 0 and 50 cm, respectively. The resulting values of the soil depth $nsoil_i$ for each vegetation type i are compiled in Table 1. To obtain the soil depth $nsoil(x,y)$ of a grid cell, the soil depth $nsoil_i$ is weighted by the relative coverage of each vegetation type $p_i(x,y)$ in the cell. The soil depth $nsoil(x,y)$, in cm, is then calculated from:

$$nsoil(x, y) = \frac{\sum_{i=1}^7 p_i(x, y) \cdot nsoil_i}{\sum_{i=1}^7 p_i(x, y)} . \quad (7)$$

The resulting global distribution of soil depth in wetlands is shown in Figure 4c. Estimates or measurements of the active layer depth lie in the same order of magnitude as the n_{soil} values derived by this method [Walter and Heimann, 2000].

3. 6. Relative Pores Space, f_{coarse}

The relative pore space of a soil is determined using the global data set of soil profiles by Dunne and Willmott [1996]. This data set, at a resolution of 0.5° by 0.5° , is based on two soil data sets [Gildea and Moore, 1985; Zabler, 1986], both of which are digital versions of the FAO/Unesco soil maps [FAO/Unesco, 1971-1981]. In the data set of Dunne and Willmott [1996], each soil profile is divided in 4 horizons each with information on soil texture and thickness. Soil texture is expressed in terms of sand, silt and clay content, and organic soils are also included. In the model, the relative pore space is used to calculate diffusion of methane through soil. Therefore, the fraction of large, air-filled soil pores is needed. Thus, f_{coarse} is determined from the fraction of coarse pores $f_{coarse,j}$ for each horizon j :

$$f_{coarse,j} = f_{sand,j} \cdot p_{v_{sand}} + f_{silt,j} \cdot p_{v_{silt}} + f_{clay,j} \cdot p_{v_{clay}} + f_{org,j} \cdot p_{v_{org}} , \quad (8)$$

where $f_{sand,j}$, $f_{silt,j}$, $f_{clay,j}$ and $f_{org,j}$ denote the relative contents of sand, silt, clay and organic material in each soil horizon j , respectively. $p_{v_{sand}}$, $p_{v_{silt}}$, $p_{v_{clay}}$ and $p_{v_{org}}$ indicate the relative volume of coarse pores in sandy, silty, clayic and organic soils, respectively. Based on Hartge and Horn [1991] they are set to 0.45, 0.20, 0.14 and 0.45, respectively. The parameter f_{coarse} is then obtained by averaging the $f_{coarse,j}$ values of all soil horizons. The obtained f_{coarse} values are transformed from a 0.5° by 0.5° grid to a 1° by 1° grid by averaging. The global distribution of f_{coarse} thus obtained is shown in Figure 4d for all wetland grid cells.

4. The Hydrologic Model

For this research, a wetland is characterized by a water table at or near the soil surface for a significant part of the year. In general, inflow and outflow of water are balanced on an annual time scale, although, there can be strong seasonal or interannual variations. Input of water includes precipitation, lateral surface or subsurface inflow, and flooding rivers or tides, while outflow can be surface or subsurface outflow and evapotranspiration [Mitsch and Gosselink, 1993]. Climate and topography play a major role; for example, level areas and depressions are favored, and very moist soil conditions lead to slow decomposition rates and hence to the accumulation of organic matter.

The movement of water through soils is affected by gravity and the capillary forces governed by the soil matrix and can be described using two criteria, hydraulic conductivity and water retention characteristics. The hydraulic conductivity depends on the size, form and continuity of pores in the soil [e.g. *Hartge and Horn*, 1991] and, in general, is higher in soils with larger pores. Hydraulic conductivity is also a function of the soil water content and increases with increasing soil moisture. Wetlands are characterized not only by high soil moisture but often by very porous soils, because they generally contain large fractions of organic matter. Therefore, they usually have high hydraulic conductivity. The ability of soil to retain water depends mainly on the pore size distribution. In organic soils, the pore size distribution is affected by the decomposition stage of the soil. Normally, in a wetland, the uppermost layer consists of slightly decomposed peat (fibric peat), the medium layer consists of moderately decomposed peat (hemic peat), and in the deepest layer the soil is well decomposed (sapric peat) [*Boelter*, 1968; *Mitsch and Gosselink*, 1993]. In general, less decomposed soils have larger pores and therefore retain less water. Hence, the ability to retain water increases with depth. In this context, the water yield coefficient [*Boelter*, 1968] is a useful parameter since it is a measure of the quantity of water removed from a peat profile when the water table is lowered. It is defined as volume of water, per soil volume, that is removed when the water table is lowered. The water yield coefficient has been found to vary between 0.08 and 0.85 (volume of water/volume of soil) for well decomposed and undecomposed soils, respectively [*Boelter*, 1968].

4. 1. Model Description

The hydrologic model is built to simulate fluctuations of the water table in wetlands as a function of climate. The position of the water table is calculated on a daily basis using a simple water balance equation. The model forcing comprises daily data on total precipitation and 2m-(air-)temperature and 6-hourly data of surface solar net radiation. The spatial resolution is 1° by 1° . It is assumed that hydraulic conductivity is high and that water retention potential increases with depth. Therefore, the wetland soil is considered as a simple, modified bucket. This modified bucket, shown schematically in Figure 5, differs from bucket models commonly used for mineral soils and has the following properties. (1) The bucket volume is considered to be the soil pore space between field capacity (originally defined as the amount of water remaining in the soil after the downward movement under gravity has largely ceased [*Veihmeyer and Hendrickson*, 1931]) and saturation, which means the wetland soil is assumed to be at field capacity at all depths and the hydrologic model calculates where the soil is saturated. (2) It is assumed that the soil is permanently water-saturated below a certain depth which is set to the soil depth n_{soil} . This means that the modified bucket has a lower boundary, n_{soil} , across which no drainage of water occurs. (3) The modified bucket is full below the

water table and empty above it. (4) The modified bucket gets smaller with depth; i.e., the water yield coefficient decreases with depth taking into account that the soil is stratified and the water retention potential increases with depth.

The total volume of the bucket, V_{tot} , is calculated using the water yield coefficient, C_{wy} . Based on values reported by *Boelter* [1968] the following values for C_{wy} are chosen: 0.8 at the soil surface, 0.26 at 20 cm depth and 0.13 at 100 cm depth, and C_{wy} is linearly decreasing between those values (Figure 5). V_{tot} is assumed to be larger in soils with a larger relative pore space f_{coarse} . Hence the function $f_{\text{wy}}(z)$ describing the amount of water removed from depth z when the water table is lowered below depth z is defined by

$$f_{\text{wy}}(z) = C_{\text{wy}}(z) \cdot \frac{f_{\text{coarse}}}{f_{\text{coarse,max}}} , \quad (9)$$

where f_{coarse} is the relative volume of coarse pores at a grid cell and $f_{\text{coarse,max}}$ is the maximum global value of f_{coarse} . $C_{\text{wy}}(z)$ denotes the variation of C_{wy} as a function of depth z . Using $f_{\text{wy}}(z)$, V_{tot} is calculated by integrating over the whole soil depth

$$V_{\text{tot}} = \int_{\text{nsoil}}^{\text{ns}} f_{\text{wy}}(z) dz , \quad (10)$$

where nsoil is the lower boundary of the bucket and ns the soil surface. The unit of V_{tot} is cm (multiply by respective wetland area to get a volume). The hydrologic model is initialized with a full bucket and run to equilibrium, so that results are independent of initial conditions.

The following ways of inflow and outflow of water are considered. Input of water can be precipitation and lateral inflow, and removal of water occurs by evapotranspiration and runoff. There is currently no distinction between lateral surface and sub-surface flow. Since wetlands usually form under conditions where lateral outflow is inhibited (e.g. by topography), only surface runoff is considered. Lateral inflow is taken into account only in arid regions. The volume of water stored in the bucket, V_{wat} , is calculated daily, and day-to-day changes in V_{wat} are calculated solving the water balance equation

$$\frac{d}{dt} V_{\text{wat}} \text{wat}(t) = P(t) - ET(t) + L(t) - R(t) , \quad (11)$$

where $P(t)$ denotes precipitation, $ET(t)$ evapotranspiration, $L(t)$ lateral inflow of water and $R(t)$ surface runoff. $P(t)$, $ET(t)$, $L(t)$ and $R(t)$ are given in cm d^{-1} while the unit of $V_{\text{wat}}(t)$ is cm.

4. 1. 1. Evapotranspiration

Evapotranspiration includes evaporation from the soil surface and transpiration by plants. The actual evapotranspiration rate is limited by the supply of water from the soil. Hence, $ET(t)$ is calculated from:

$$ET(t) = \min(\text{demand}(t), \text{supply}(t)) . \quad (12)$$

$\text{Supply}(t)$ denotes the actual evapotranspiration rate restricted by availability of water in the soil. $\text{Demand}(t)$ is calculated using the equilibrium evapotranspiration rate derived from the energy balance between net radiation, latent and sensible heat fluxes and ground heat flux at the soil surface. Assuming that the ground heat flux is small compared to the latent and sensible heat fluxes, $\text{demand}(t)$ is calculated after *Jarvis and McNaughton* [1986]:

$$\text{demand}(t) = \frac{s_T(t)}{s_T(t) + \gamma} \cdot \frac{\text{rad}(t)}{\lambda} , \quad (13)$$

where λ is the latent heat of evaporation (2.45 MJ kg^{-1} at 20°C) and γ the psychrometric constant of about 65 Pa K^{-1} . $\text{Rad}(t)$ denotes the net radiation at the soil surface calculated as the sum of the surface solar and thermal radiation. $s_T(t)$ denotes the temperature derivative of the saturation vapor pressure curve, de_s/dT , whereby the saturation vapor pressure e_s is calculated after the Mangus formula [e.g. *Murray*, 1967]. Hence, $s_T(t)$ yields:

$$s_T(t) = \lambda \cdot \frac{e^{\frac{l_1 \cdot T_{2m}(t)}{l_2 + T_{2m}(t)}}}{l_2 + T_{2m}(t)^2} , \quad (14)$$

where $T_{2m}(t)$ is the air temperature at 2m height and l_1 and l_2 are constants which are 17.269 and 237.3, respectively. If the soil does not contain enough water to evaporate at the equilibrium evapotranspiration rate, the actual evapotranspiration rate is calculated after *Federer* [1982]:

$$\text{supply}(t) = c \cdot \frac{V_{\text{wat}}(t)}{V_{\text{tot}}} , \quad (15)$$

where V_{tot} is the maximum bucket size and $V_{\text{wat}}(t)$ the volume of water stored in the bucket at time t . C is a factor (cm d^{-1}) that depends on $V_{\text{wat}}(t)$ and the relative vegetation coverage of the soil:

$$c = \begin{cases} 1.5 & \text{if}(V_{\text{wat}}(t) \geq V_{\text{tot}}) \\ 0.24 + 0.96 \cdot \frac{100 - p_{\text{bare}}}{100} & \text{else} \end{cases}, \quad (16)$$

where p_{bare} denotes the percentage of unvegetated, bare soil which is derived from the global land cover data set by *Wilson and Henderson-Sellers* [1985]. Maximum supply rates of 1.5 cm d^{-1} are used for grid cells with standing water (i.e., if $V_{\text{wat}}(t) \geq V_{\text{tot}}$), while 0.24 cm d^{-1} and 1.2 cm d^{-1} are used for unvegetated and for totally vegetated grid cells, respectively, according to *Kaduk* [1996].

4. 1. 2. Lateral Inflow

Some wetlands occur in arid regions where wetlands would not be located if precipitation were the only source of water (Figure 3). In the hydrologic model, a region is defined to be arid, if the difference between total annual precipitation and total annual potential evapotranspiration (PmE) is negative. These wetlands are most likely fed by lateral inflow of water from higher lands, lakes and/or rivers, the Niger and the Parana are examples of these arid wetlands. In order to maintain wetland conditions, the annual inflow of water to a wetland must be equal or greater than the annual outflow. Therefore, the lateral inflow $L(t)$ is introduced to close the water balance in regions where PmE is negative. For the sake of simplicity, potential sources of lateral inflow, such as higher lands, rivers or lakes, are not distinguished. The different origins of lateral inflow would affect its seasonality. Instead, the amount of water needed to close the annual PmE balance is added to the bucket at a constant daily rate throughout the year. Hence, $L(t)$ is calculated from:

$$L(t) = \begin{cases} 0 & \text{if}(PmE > 0) \\ \frac{-PmE}{\text{days}} & \text{else} \end{cases}, \quad (17)$$

where days denotes the number of days of the year. The parameterization of $L(t)$ constitutes a strong simplification. However, since only wetlands are considered, $L(t)$, if not zero, is small compared to the other components of Equation 6. In reality, there is also lateral inflow of water in non-arid regions. In the hydrologic model, however, this is compensated for by higher runoff, since the model is run in equilibrium on an annual basis. Therefore, ignoring lateral inflow in non-arid regions does not affect simulated water table levels very much.

4. 1. 3. Runoff

It is assumed that wetlands are typically located in regions where lateral drainage is inhibited. Therefore, only surface runoff, $R(t)$, is considered. In the hydrologic model runoff occurs only in conditions of standing water, i.e. if $V_{\text{wat}}(t) > V_{\text{tot}}$. The amount of outflow via runoff is assumed to depend on the height of the standing water and the terrain steepness. It is calculated from:

$$R(t) = \begin{cases} 0 & \text{if } (V_{\text{wat}}(t) < V_{\text{tot}}) \\ H_{\text{wt}}(t) \cdot \left\{ \frac{H_{\text{wt}}(t)^2}{k_1} + \frac{S}{k_2} \right\} & \text{else} \end{cases} \quad (18)$$

S is the Laplace operator of the terrain height, i.e. $S=|\Delta \text{terrain height}|$, which is derived from the 5' by 5' topographical data set ETOPO5 [Edwards, 1989] and interpolated to the 1° by 1° resolution. $H_{\text{wt}}(t)$ is the height of the water table relative to the soil surface in cm and k_1 and k_2 are constants, which are set to 1500 d cm^2 and 2000 d , respectively. k_1 and k_2 are chosen in such that (1) ~50-90% of the standing water is removed daily by runoff and (2) influences of $H_{\text{wt}}(t)$ and the terrain slope, S , on runoff are balanced in situations with average values for S and $H_{\text{wt}}(t)$ (~10cm). Sensitivity tests have shown that the results of the hydrologic model are not very sensitive to the choice of k_1 and k_2 [Walter, 1998].

4. 2. Results and Discussion

4. 2. 1. Tests against observational data

The hydrologic model simulates the position of the water table in the wetland fraction of a 1° by 1° grid cell. A single “mean” water table level is calculated for the wetland fraction of cells, thereby neglecting that soils are heterogeneous and the position of the water table usually varies within a wetland due to microtopography. The possible effects of neglecting microtopography on simulated methane emissions is tested and discussed in sections 3.4.2 and 3.5 of Walter *et al.* [this issue]. For the test against water table observed at field sites, the required inputs for the hydrologic model (precipitation, surface solar net radiation and 2m-temperature) were not available. Therefore, ECMWF reanalyses [Gibson *et al.*, 1997] were used as forcing (section 2 of Walter *et al.* [this issue]). Since the variability of the input data, particularly precipitation, within one grid cell is usually quite high, the ECMWF input data probably differ from the actual input data at the respective sites. Hence, a more rigorous test of the hydrologic model would include field input data. However, in a test using reanalyses it can be examined if seasonal patterns and the magnitude of observed water table fluctuations can be reproduced.

Water table data are available from the test sites of the methane model [Walter and Heimann, 2000]. Observed water table levels are compared to simulated water table levels of the grid cell where the test site is located. Figure 6 shows the results at four sites located in Finland and the US (Alaska, Minnesota and Michigan). The observations are from Saarnio *et al.* [1997] (Finland), Whalen and Reeburgh [1992] (Alaska), Dise [1993] (Minnesota) and Shannon and White [1994] (Michigan). At most sites measurements at several different microsites within the wetland were performed. The data show that within one site water table levels can differ by several tens of centimeters between hummock and hollow structures, for example, at the sites in Finland and Minnesota. The seasonal patterns and magnitudes of water table fluctuations are reproduced reasonably by the hydrologic model at most sites. However, at the Minnesota and Michigan sites, the amplitude of simulated water table levels is overestimated. This could be due to the form of the function $C_{wy}(z)$, which decreases strongly from the soil surface to 20 cm soil depth and is small below -20 cm. Hence, below 20 cm soil depth, the removal of a fixed amount of water translates into a much bigger decline in water table than in the upper 20 cm of soil. This could explain the sharp decrease in simulated water table levels in Figure 6c and Figure 6d. The global model runs combining the hydrologic and methane models were performed using this version of the hydrologic model. In the future, different formulations of $C_{wy}(z)$ should be tested in order to further improve the hydrologic model. Figure 5 of Walter *et al.* [this issue] shows another comparison of simulated water tables with observations.

4. 2. 2. Sensitivity Tests

The sensitivity of the hydrologic model to changes in the parameters k_1 and k_2 and in precipitation was evaluated. Model results are not very sensitive to k_1 and k_2 , whether or not standing water occurs rarely or often, nor how high the water table is above the soil surface [Walter, 1998]. The results of the sensitivity test to changes in precipitation are shown in Figure 7 for six grid cells from different regions representing a variety of soil and climatic conditions. The model was forced with ECMWF reanalyses for 1988 (section 2 of Walter *et al.* [this issue]). Three runs were performed using 100% precipitation (control), 80% precipitation, and 120% precipitation. Greater precipitation generally leads to higher water table levels and vice versa, but the relative effect of a 20% increase or decrease in precipitation varies among sites. For example, the effect is large at the Alaskan and the Finish sites, but small at the Minnesotan or Michigan sites. In general, a $\pm 20\%$ change in precipitation has a smaller effect at sites where precipitation is higher, and vice versa [Walter, 1998]. Therefore, the effect is smaller at most tropical sites as, for example, in Panama (see also Figure 8). In the tropics precipitation is extremely low during the dry season and a $\pm 20\%$ change does not change much; during the wet season precipitation is very high causing standing water, and a $\pm 20\%$

change only changes the amount of run-off. However, in some tropical regions greater precipitation can cause lower water table levels, and vice versa (Chad). This occurs in arid regions, where PmE is negative and the lateral inflow, L , (Equation 17) is different from zero. L is calculated every year and is smaller in years with greater precipitation, and vice versa. Different L values due to different precipitation affect the water table mainly during the dry season. Since most methane emissions take place in the wet season it is not expected to change modeled methane emissions very much (see also section 3.4.2 of *Walter et al.* [this issue]). However, this problem will be fixed in future versions of the model.

The results of the same sensitivity test ($\pm 20\%$ precipitation) are plotted globally as annual means in Figure 8. At most places reduced precipitation leads to lower annual water table levels, and vice versa. The arid regions where owing to the parameterization of the lateral inflow, L , the opposite happens are some regions in Africa and South America. Considering only those places where changes in precipitation and water table have the same sign, Figure 8 shows that $\pm 20\%$ changes in precipitation have a stronger effect in the HNH than in the tropics as explained in the last paragraph.

4. 2. 3. The Water Table in Wetlands and its Seasonality

Figure 9 shows global results of the hydrologic model for wetland points only. Monthly mean water table levels are plotted for February, May, August and November. In higher northern hemisphere ($> 30^\circ N$, HNH) wetlands the water table is high during the winter and low during the summer. In tropical wetlands the water table is low during the dry season, which last from February to May in northern hemisphere tropics and from August to November in southern hemisphere tropics. The amplitudes of variations in the water table are generally larger in the tropics with standing water during the wet season and water levels below 1 m soil depth (Figure 7, Panama) during the dry season.

4. 2. 4. Hydrologic Model: Limitations

Although the hydrologic model is a relatively simple approach, the results of the comparison between modeled and observed water table levels illustrate that it yields realistic results. As discussed in sections 4.2.1 and 4.2.2 different choices of the function $C_{wy}(z)$ should be tested and the parameterization of the lateral inflow, L , should be improved in the future. In addition, the following three factors that are not yet considered may be important: (1) the contribution of permafrost, (2) snow, and (3) wetland microtopography. (1) In permafrost soils water is stored in the form of ice until the soils thaw. Furthermore, surface water cannot infiltrate into a frozen soil. Both facts favor saturation of surface soils in spring. While the hydrologic model

performs well at the Alaskan site, which is underlain by permafrost, further tests with data from other permafrost sites should be conducted. (2) Water is also stored in the form of snow until the snow melts. This also favors saturation of surface soils in spring. However, the model results do not differ systematically from observations in spring. (3) The position of the water table calculated by the hydrologic model can be viewed as a “mean” water table level of a wetland. However, complex microtopography can result in water table levels that vary by several tens of centimeters on small spatial scales (i.e., in the order of meters). The methane model is quite sensitive to the position of the water table mostly due to efficient oxidation of methane in oxic surface soils. Therefore, neglecting the effects of microtopography on water table can affect modeled methane emissions as discussed in sections 3.4.2 and 3.5 of *Walter et al.* [this issue]. Hence microtopography should be included into future version of the hydrologic model.

5. Summary and Conclusion

In this article we presented the components of a global, process-based, climate-sensitive methane-hydrology model to derive methane emissions from natural wetlands. As the processes controlling methane production rates are not modeled explicitly, a simple method to derive spatial variations in the production rate (i.e., in R_0 of Equation 1) from annual NPP and soil temperature was developed. In the future, a model to derive R_0 from biogeochemical, biogeographical and climatic variables could be used to replace Equation 2. However, in order to do so more needs to be known about quantitative relationships between these parameters and R_0 , and data on the global distribution of factors affecting R_0 need to become available.

The model was applied to the global wetland distribution of *Matthews and Fung* [1987]. Global data sets of all model parameters - efficiency of plant-mediated transport, rooting depth, soil depth, and relative pore space - were developed from existing global data sets of vegetation [*Wilson and Henderson-Sellers*, 1985] and soil characteristics [*Dunne and Wilmott*, 1996]. Efficiency of plant-mediated transport was derived from the still sparse knowledge about the gas conducting properties of different plants. Rooting depth and soil depth were determined from vegetation related vertical distributions of root biomass. Relative pore space was derived from a global data set on soil texture. All these parameters are not homogeneously distributed within a 1° by 1° grid-cell and few data sets consider the special conditions prevailing in wetlands. Hence, higher resolution data sets might help to improve global data sets of the model parameters in the future.

A simple hydrologic model to derive the variation of the water table in wetlands was

developed. The model is based on assumptions made for wetland conditions. No data set comprising input and output data of the model has been available. Therefore, simulated variations in the water table of a grid-cell were compared to point measurements obtained within the same grid-cell. Nonetheless the limitations of this comparison, it could be shown that the hydrologic model calculates realistic seasonal cycles in the water table. Different variations of the water yield coefficient ($C_{wy}(z)$ in Equation 9) should be tested in the future. A sensitivity test of the hydrologic model showed that the effect of a $\pm 20\%$ change in precipitation varies between different sites. In general, greater precipitation leads to higher water levels, and vice versa, and the effect of a $\pm 20\%$ change in precipitation is higher in HNH wetlands. However, in regions where the difference between total annual precipitation and total annual potential evapotranspiration (PmE) is negative, this opposite can be the case. In these regions lateral inflow (L in Equation 17), which is inversely related to precipitation, is different from zero. Hence, lower precipitation can lead to higher water table which occurs in some African and South American wetlands. Since this effect occurs mainly during the dry season it is not expected to have a large impact on modeled methane emissions. However, it will be fixed in future versions of the hydrologic model. Simulated water levels in HNH wetlands are highest during the winter and lowest during the summer. In the tropics, there is usually standing water during the wet season and very low (often below 1 m soil depth) water levels during the dry season. The amplitude of seasonal variations in the water table is, in general, larger in tropical wetlands. Owing to microtopography the position of the water table relative to the soil surface is not constant throughout a wetland. This effect has not yet been considered in the hydrologic model and should be included in future versions.

In summary, different components have been developed in order to apply a well-tested process-based model to derive global methane emissions from natural wetlands. There are still limitations in the knowledge about processes and/or the availability of global data sets which cause limitations in the model. However, this global methane-hydrology model constitutes a tool to study climate-induced variations in methane emissions from global wetlands.

Acknowledgments. Many thanks to Nigel Roulet and Matt Letts for informative discussions concerning the hydrologic model. In addition, B. Walter would like to thank Peter Frenzel for discussions regarding vegetation and transport. This work was supported by the German Bundesministerium für Bildung, Wissenschaft, Forschung und Technologie (BMBF) as part of the Klimaschwerpunkt "Spurenstoffkreisläufe" and, in part, by NASA's Atmospheric Chemistry Program.

References

Boelter, D. H., Important physical properties of peat materials, In: *Proceedings of the Third International Peat Congress, Quebec City, Quebec, Aug. 18-23, 1968, Department of Energy, Mines and Resources Canada. National Research Council of Canada*, 1968.

Cao, M., S. Marshall, K. Gregson, Global carbon exchange and methane emission from natural wetlands: Application of a process-based model, *J. Geophys. Res.*, *101*, D9, 14399-14414, 1996.

Dise, N. B., Methane emission from Minnesota peatlands: Spatial and Seasonal Variability, *Global Biogeochem. Cycles*, *7*, 1, 123-142, 1993.

Dlugokencky, E. J., K. A. Masarie, P. M. Lang, P. P. Tans, Continuing decline in the growth rate of atmospheric methane, *Nature*, *393*, 447-450, 1998.

Dunne, K. A., C. J. Willmott, Global distribution of plant-extractable water capacity of soil, *International Journal of Climatology*, *16*, 16841-16859, 1996.

Edwards, M. O., Global gridded elevation and bathymetry (ETOPO5). Digital raster data on a 5-minute geographic (lat/lon) 2160*4320 (centroid-registered) grid. *NOAA National Geophysical Data Center, Boulder, Colorado*, 1989.

FAO/Unesco, 1971-1981: Soil map of the world, Vols. 1-10, *Unesco, Paris*.

Federer, C. A., Transpirational supply and demand: Plant, soil, and atmospheric effects evaluated by simulation, *Water Resour. Res.*, *18*, 355-362, 1982.

Gale, M. R., D. F. Grigal, Vertical root distributions of northern tree species in relation to successional status, *Canadian Journal of Forest Research*, *17*, 829-834, 1987.

Gibson, J. K., P. Källberg, S. Uppala, A. Hernandez, A. Nomura and E. Serrano, The ECMWF Re-Analysis (ERA). 1. ERA description, *ECMWF Re-Analysis Project Report Series No. 1, European Centre for Medium-Range Weather Forecasts, Reading, U.K.*, 71 pp, 1997.

Gildea, M. P., B. Moore, FAOSOL - A global soil archive, *Complex systems research center*,

University of New Hampshire, Durham, New Hampshire (unpublished data tape and documentation), 1985.

Hartge, K. H., R. Horn, Einführung in die Bodenphysik, *Ferdinand Enke Verlag, Stuttgart*, 1991.

Hogan, K., R. Harriss, Comment on „A dramatic increase in the growth rate of atmospheric methane in the northern hemisphere during 1992“, by E. J. Dlugokencky et al., *Geophys. Res. Lett.*, Vol. 21, 2445-2446, 1994.

Jackson, R. B., J. Canadell, J. R. Ehleringer, H. A. Mooney, O. E. Sala, E. D. Schulze, A global analysis of root distributions for terrestrial biomes, *Oecologia*, 108, 3, 389-411, 1996.

Jarvis, P. G., K. G. McNaughton, Stomatal control of transpiration: Scaling up from leaf to region, *Adv. Ecol. Res.*, 15, 1-49, 1986.

Jouzel, J., N. I. Barkov, J. M. Barnola, M. Bender, J. Chappellaz, C. Genthon, V. M. Kotlyakov, V. Lipenkov, C. Lorius, J. R. Petit, D. Raynaud, G. Raisbeck, C. Ritz, T. Sowers, M. Stievenard, F. Yiou, P. Yiou, Extending the Vostock ice-core record of paleoclimate to the penultimate glacial period, *Nature*, 364, 407-412, 1993.

Kaduk, J., Simulation der Kohlenstoffdynamik der globalen Landbiosphäre mit SILVAN - Modellbeschreibung und Ergebnisse, *Dissertation, Max-Planck-Institut für Meteorologie, Examensarbeit Nr. 42*, 1996.

Knorr, W., Satellite remote sensing and modelling of the global CO₂ exchange of land vegetation: A synthesis study, dissertation, Examensarbeit 49, Max-Planck-Inst. für Meteorol., Hamburg, Germany, 1997.

Lelieveld, J., P. J. Crutzen, F. J. Dentener, Changing concentration, lifetime and climate forcing of atmospheric methane, *Tellus*, 50B, 128-150, 1998.

Matthews, E., I. Fung, Methane emission from natural wetlands: Global distribution, area, and environmental characteristics of sources, *Global Biogeochem. Cycles*, Vol. 1, No. 1, 1987.

Mitsch, W. J., J. G. Gosselink, Wetlands, *Van Nostrand Reinhold, New York*, 1993.

Murray, F. W., On the computation of saturation vapour pressure, *J. Appl. Meteorol.*, 6, 203-204, 1967.

Ramachandran, P., Ramachandran R., Methane emission inventory from tropical coastal wetlands (Mangrove ecosystems), poster presented at the *Joint International Symposium on Global Atmospheric Chemistry (CACGP and IGAC)*, Seattle, WA, 1998.

Saarnio, S., J. Alm, J. Silvola, A. Lohila, H. Nykänen, P. J. Martikainen, Seasonal variation in CH₄ emissions and production and oxidation potentials at microsites of an oligotrophic pine fen, *Oecologia*, 110, 414-422, 1997.

Schimel, J. P., Plant transport and methane production as controls on methane flux from arctic wet meadow tundra, *Biogeochemistry*, 28, 183-200, 1995.

Schütz, H., W. Seiler, R. Conrad, Processes involved in formation and emission of methane in rice paddies, *Biogeochemistry*, 27, 35-60, 1989.

Severinghaus, J.P., T. Sowers, E.J. Brook, R.B. Alley, M.L. Bender, Timing of abrupt climate change at the end of the Younger Dryas interval from thermally fractionated gases in polar ice, *Nature*, 391, 141-146, 1998.

Severinghaus, J.P., E.J. Brook, Abrupt climate change at the end of the last glacial period inferred from trapped air in polar ice, *Science*, 286 (5441), 930-934, 1999.

Shannon, R. D., J. R. White, A three-year study of controls on methane emissions from two Michigan peatlands, *Biogeochemistry*, 27, 35-60, 1994.

Shannon, R. D., J. R. White, J. E. Lawson, B. S. Gilmour, Methane efflux from emergent vegetation in peatlands, *Journal of Ecology*, 84, 2, 239-246, 1996.

Valentine, D. W., E. A. Holland, D. S. Schimel, Ecosystem and physiological controls over methane production in northern wetlands, *J. Geophys. Res.*, 99, D1, 1563-1571, 1994.

Veihmeyer, F.J., A.H. Hendrickson, The moisture equivalent as a measure of the field capacity of soils, *Soil Sci.*, 32, 181-193, 1931.

Walter, B. P., M. Heimann, R. D. Shannon, J. R. White, A process-based model to derive

methane emissions from natural wetlands, *Geophys. Res. Lett.*, 23, 25, 3731-3734, 1996.

Walter, B.P., Development of a process-based model to derive methane emissions from natural wetlands for climate studies, dissertation, Examensarbeit 60, Max-Planck-Inst. für Meteorol., Hamburg, Germany, 1998.

Walter, B.P., M. Heimann, A process-based, climate-sensitive model to derive methane emissions from natural wetlands: Application to five wetland sites, sensitivity to model parameters, and climate, *Global Biogeochem. Cycles*, in press, 2000.

Walter, B.P., M. Heimann, E. Matthews, Modeling modern methane emissions from natural wetlands, 2. Interannual Variations 1982-1993, *J. Geophys. Res.*, this issue.

Whalen, S. C., W. S. Reeburgh, Interannual variations in tundra methane emissions: A four-year time series at fixed sites, *Global Biogeochem. Cycles*, 6, 139-159, 1992.

Wilson, M. F., A. Henderson-Sellers, A global archive of land cover and soils data for use in general circulation models, *Journal of Climatology*, 5, 119-143, 1985.

Zobler, L., A world soil file for global climate modeling, *National Aeronautics and Space Administration, Washington, DC, NASA, Technical Memorandum, 87802*, 1986.

Table 1: Parameters T_{veg} , n_{root} , and n_{soil} for each vegetation type

This study's vegetation types		$T_{veg,i}$	n_{root_i} (cm)	n_{soil_i} (cm)
0	other	0	0	0
1	tree	1	64	129
2	shrub	0	63	126
3	short grass	10	39	79
4	long grass	15	81	162
5	tundra	10	26	51
6	swamp	15	39	79
7	bare soil	0	0	50

Table 2: Vegetation types and extinction coefficient β

This study's vegetation types		<i>Jackson et al.</i> 's vegetation types	β
1	tree	boreal forest	0.943
		temperate coniferous forest	0.977
		temperate deciduous forest	0.966
		tropical deciduous forest	0.961
		tropical evergreen forest	0.962
2	shrub	sclerophyllous shrubs	0.964
3	short grass	temperate grassland	0.943
4	long grass	tropical grassland	0.972
5	tundra	tundra	0.914
6	swamp	temperate grassland	0.943

Appendix A

As discussed in section 3.2, the 24 WH-vegetation types of the data set of *Wilson and Henderson-Sellers* [1985] are combined in this work into the following 8 vegetation types: tree, shrub, short grass, long grass, tundra, swamp, bare soil and other. The vegetation type other comprises non-natural “vegetation” types such as urban or arable lands.

Table 3: Definition of vegetation types used in this work

Types used in this work		Types by Wilson&Henderson-Sellers	
veg type	description	WH-veg type	description
0	other	1	water
		2	ice
		3	inland lake
		15	arable
		16	rice
		17	sugar
		18	maize
		19	cotton
		20	irrigated crop
		21	urban
1	tree	4	evergreen needleleaf tree
		5	evergreen broadleaf tree
		6	deciduous needleleaf tree
		7	deciduous broadleaf tree
		8	tropical broadleaf tree
		9	drought deciduous tree
2	shrub	10	evergreen broadleaf shrub
		11	deciduous shrub
		12	thorn shrub
3	short grass	13	short grass and forbs

Table 3: Definition of vegetation types used in this work

Types used in this work		Types by Wilson&Henderson-Sellers	
veg type	description	WH-veg type	description
4	long grass	14	long grass
5	tundra	22	tundra
6	swamp	23	swamp
7	bare soil	24	soil

Figure Captions:

Figure 1: Schematic of the methane model. The processes leading to methane emission to the atmosphere occur in the soil between soil depth and soil surface. Methane production takes place in the anoxic soil below the water table; the methane production rate depends on soil temperature and NPP. Methane oxidation occurs in the oxic soil above the water table and depends on temperature. The model calculates methane concentrations in each soil layer. Transport occurs by diffusion through water-/air-filled soil pores, ebullition to the water table and plant-mediated transport from layers above the rooting depth. Methane emission to the atmosphere is calculated daily.

Figure 2: Schematic of the global methane-hydrology model. The forcing of the methane model is soil temperature, NPP and water table. The water table is calculated from precipitation, 2m (air-)temperature and surface net solar radiation. The global wetland distribution is prescribed. Global data sets of the model parameters plant-mediated transport, rooting depth, soil depth, and relative pore space are used.

Figure 3: Global wetland area (10^9 m^2) as given by the data set of *Matthews and Fung* [1987].

Figure 4: Global distribution of the data sets of the model parameters. (a) Plant-mediated transport, T_{veg} ; (b) rooting depth, n_{root} (cm); (c) soil depth, n_{soil} (cm); (d) relative pore space, f_{coarse} .

Figure 5: Schematic of the hydrologic model. Input of water occurs by lateral inflow, L , and precipitation, P ; outflow of water occurs by evapotranspiration, E , and surface run-off, R . The dark grey area is the total volume of the bucket as defined by Equation 10.

Figure 6: Results of tests of the hydrologic model against data from four test sites. Modeled water tables (cm) (thick lines) and observed water tables (triangles) from (a) Finland, (b) Alaska, (c) Minnesota, and (d) Michigan. Note that y-axis units differ.

Figure 7: Sensitivity test of the hydrologic model to precipitation. Simulated water table (cm) for the control run with 100% precipitation (black), the run with 80% precipitation (dashed), and the run with 120% precipitation (grey). Note that y-axis units differ.

Figure 8: Sensitivity test of the hydrologic model to precipitation. Simulated annual mean water table (cm), difference between 80% precipitation and control (left side), and 120%

precipitation and control (right side).

Figure 9: Seasonal variation of the water table. Simulated monthly mean water table (cm) for (a) February, (b) May, (c) August, and (d) November.

Figure 1

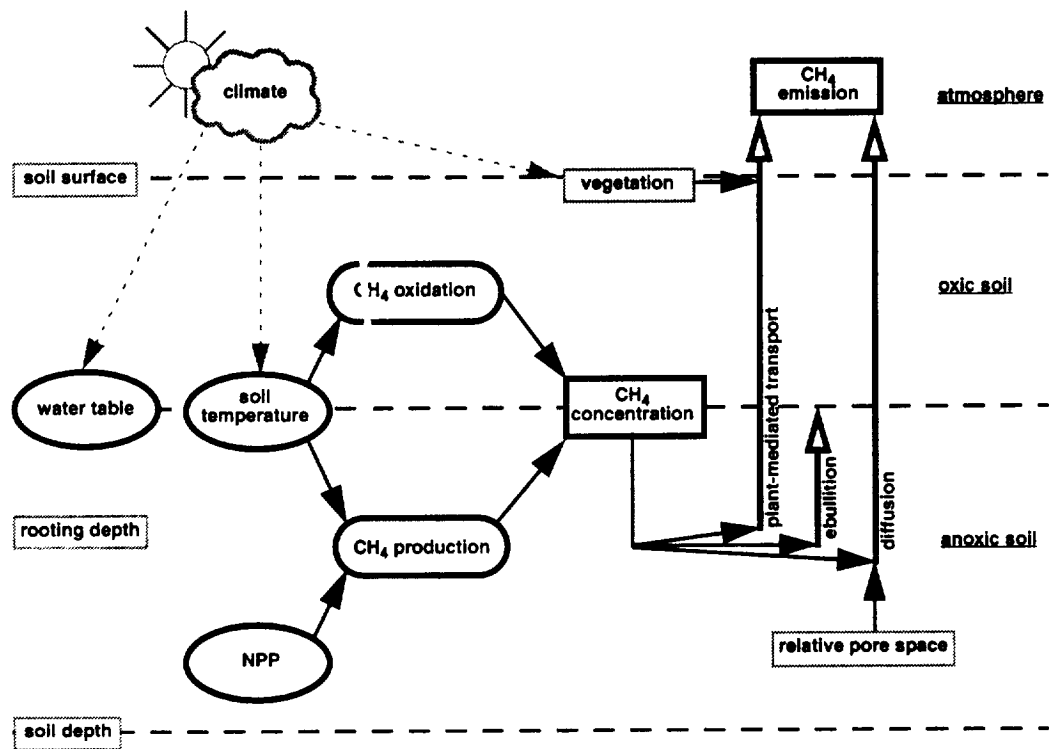


Figure 2

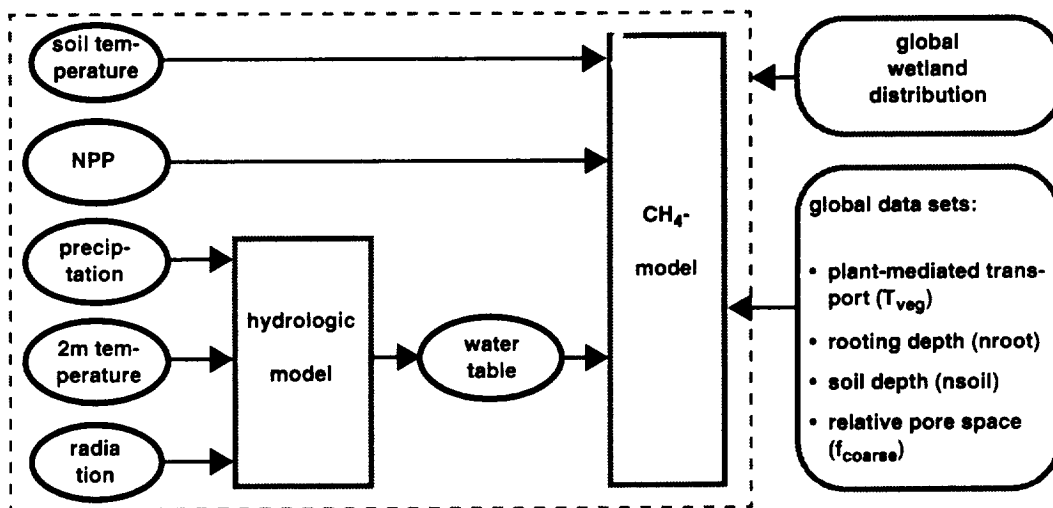


Figure 3

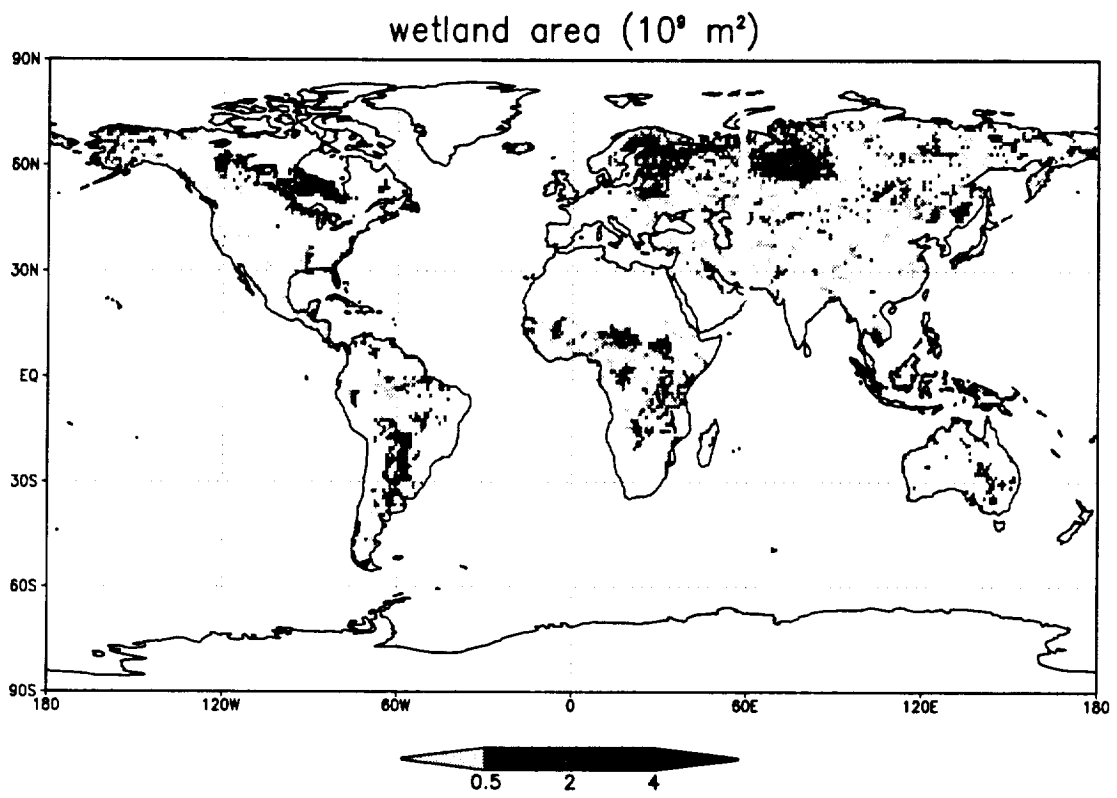


Figure 4

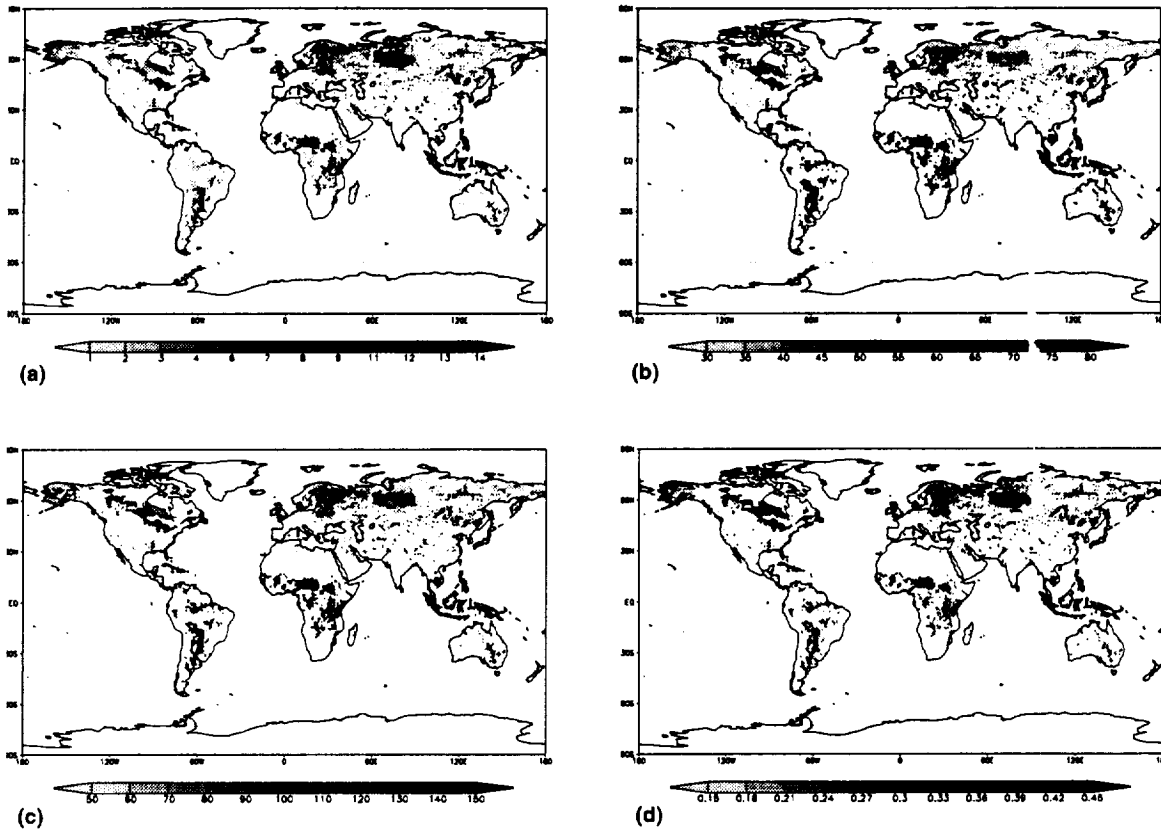


Figure 5

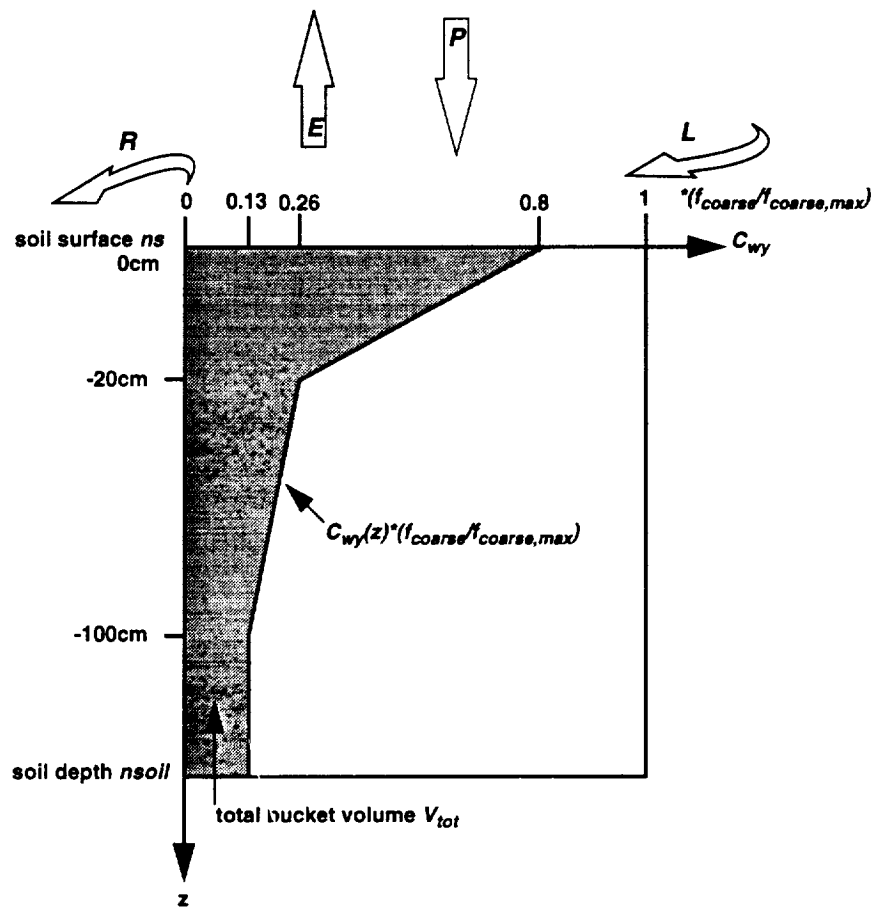


Figure 6

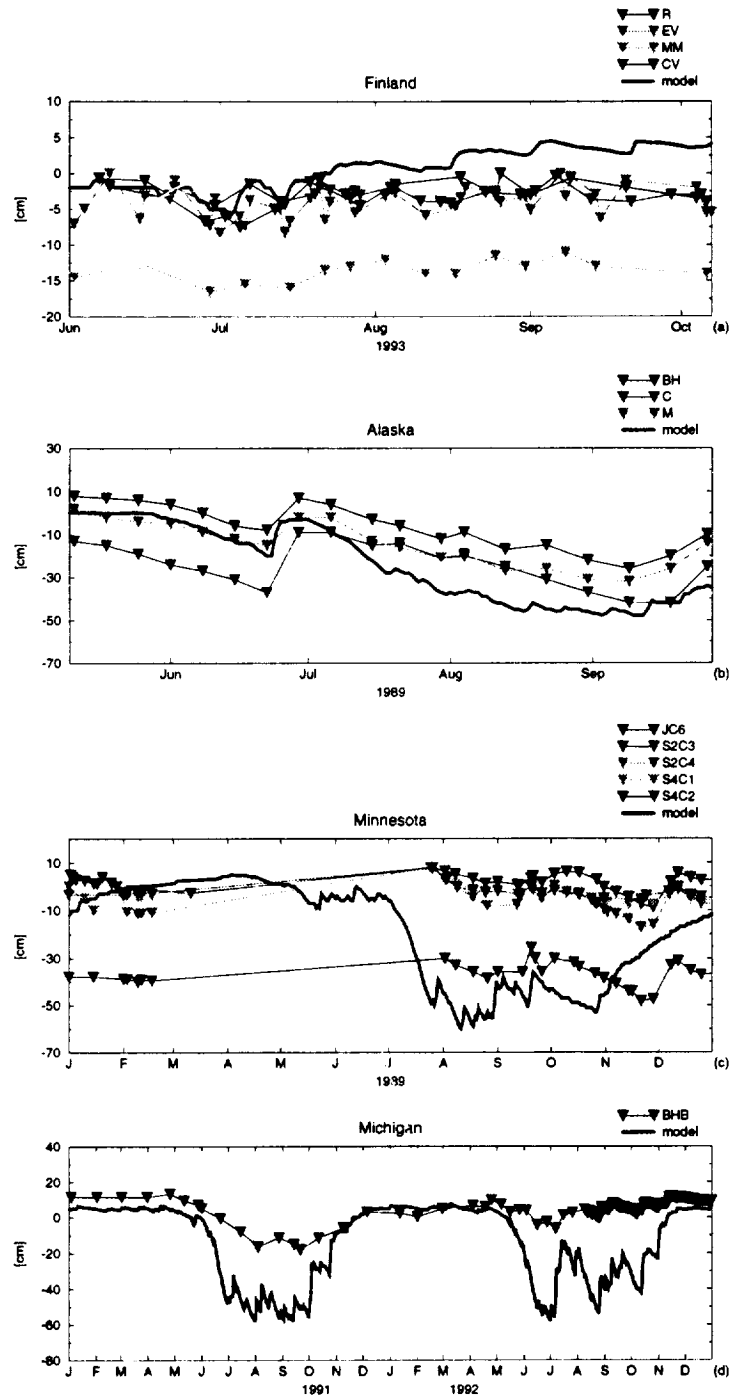


Figure 7

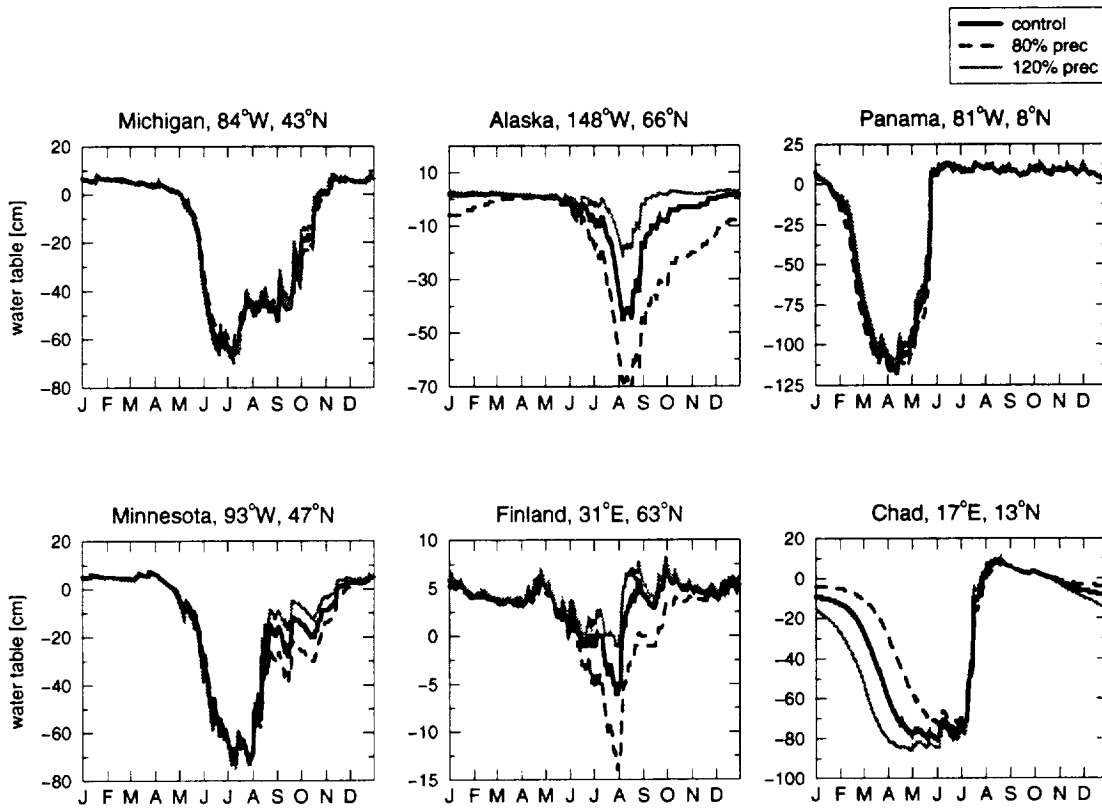


Figure 8

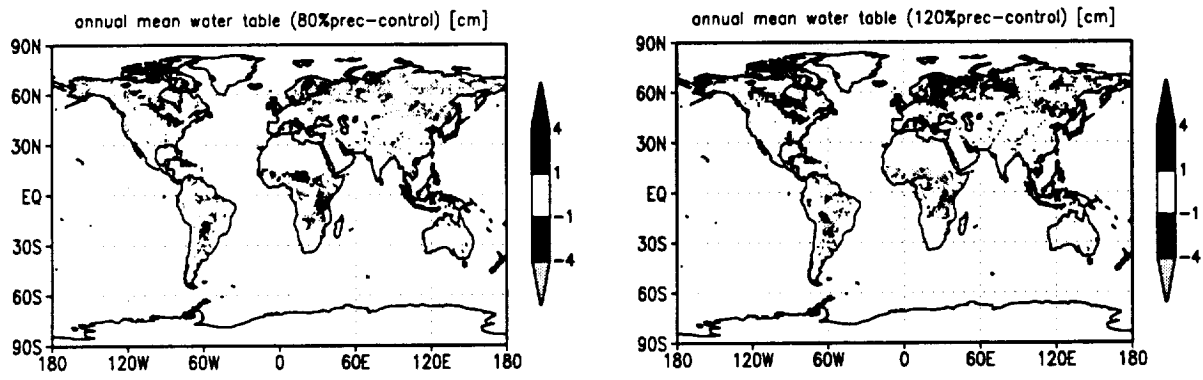


Figure 9

